LA-UR 97-1930

CONF-971005--20

Los Alamos National Laboratory is operated by the University of California for the United States Department of Energy under contract W-7405-ENG-36

TITLE: A Three-Dimensional Analytical Benchmark in a Homogeneous Semi-Infinite Medium

AUTHOR(S): Drew E. Kornreich, TSA-7
Barry D. Ganapol, University of Arizona

SUBMITTED TO: October 1997 Joint International Conference on Mathematical Methods and Supercomputing for Nuclear Applications in Saratoga Springs, New York

DISCLAIMER

Los Alamos National Laboratory
Los Alamos, New Mexico 87545

FORM NO. 836 R4
ST. NO. 2629 5/81

A THREE-DIMENSIONAL ANALYTICAL BENCHMARK IN A HOMOGENEOUS SEMI-INFINITE MEDIUM

D. E. Kornreich
Los Alamos National Laboratory
TSA-7, MS F609
Los Alamos, New Mexico 87545

B. D. Ganapol
University of Arizona
Department of Aerospace and Mechanical Engineering
Tucson, Arizona 85721

ABSTRACT

The linear Boltzmann equation for the transport of neutral particles is investigated with the objective of generating a benchmark-quality calculation for the three-dimensional searchlight problem in a semi-infinite medium. The derivation assumes stationarity, one energy group, and isotropic scattering. The surface and interior scalar fluxes are the quantities of interest. The source considered is a pencil-beam incident at a point on the surface of a semi-infinite medium. The scalar flux will have two-dimensional variation only if the beam is normal; otherwise it is three-dimensional. The solutions are obtained by using Fourier and Laplace transforms and standard numerical techniques. Comparisons of these numerical solutions to results from the probabilistic code MCNP are also provided.

I. INTRODUCTION

The scientific community continues to develop more complicated and comprehensive codes to model physical systems. These developmental codes require benchmark results with which to compare computed results to confirm that the codes are operating properly. The benchmarks generally consist of numerical results to simplified problems that a comprehensive code must be able to solve. Mathematical and numerical techniques are applied to obtain numerical results that are accurate within a desired error. Such benchmarks are called "analytical benchmarks" because they consist of numerical evaluations of analytical mathematical representations.

As the production-level codes become more comprehensive, so must the benchmarks become more comprehensive. Successively comprehensive benchmarks generally evolve from consideration of very simple problems to those that are more complex. For example, a suite of benchmarks in homogeneous isotropically scattering infinite media is established by consideration of one-dimensional problems, such as the isotropic point or isotropic plane sources, and then progresses to more complicated problems, such as anisotropic point or plane sources. The complexity may then be increased by considering semi-infinite media or slab geometries. In this paper, the development of useful benchmarks is furthered by examining a homogeneous, isotropically scattering, source-free semi-infinite medium.

One of the basic transport problems for semi-infinite media is the searchlight problem originally posed by Chandrasekhar[1] in the radiative transfer context. In the searchlight problem, radiation impinges on the free surface of a semi-infinite medium, and the resultant particle distributions are to be determined. To date, only one-group problems have been considered for a homogeneous isotropically scattering medium. The searchlight problem has been shown to be a variant of a one-dimensional pseudo problem that facilitates its solution.[2,3] Numerical analyses of the searchlight problem have been considered by Siewert and Dunn,[4,5,6] where the F_N method was applied to determine the flux from a normal beam incident on a finite slab. Elliott[7] considered an isotropic point source at the surface of a half-space, but, as would be expected from a paper of that era (1955), no numerical results were presented because of the lack of computational power. Recently,

numerical results for the searchlight problem for a half-space have been provided by Ganapol and Nigg[8] and Ganapol, *et al.*[9] for the case of a normal beam. When the beam is directed normal to the surface, the scalar flux is two-dimensional, resulting in a significant numerical advantage. However, if the beam is canted, the scalar flux is three-dimensional. This generalized case will be considered here. The analytical expressions, while complicated, will be shown to be amenable to numerical evaluation. A benchmark-type comparison between the numerical results and the production code MCNP[10] will be provided.

II. DERIVATION OF THE TRANSFORMED SCALAR FLUX

The derivation of the equations that describe the scalar flux in a semi-infinite medium for several types of surface illumination has been performed previously;[9] therefore, only a brief description of the derivation will be presented here. The simplified form of the transport equation in cylindrical coordinates is

$$\left[\mu\frac{\partial}{\partial z} + \boldsymbol{\omega}\cdot\frac{\partial}{\partial \boldsymbol{\rho}} + 1\right]\phi(z,\boldsymbol{\rho},\boldsymbol{\Omega}) = \frac{c}{4\pi}\int_{4\pi} d\boldsymbol{\Omega}'\,\phi(z,\boldsymbol{\rho},\boldsymbol{\Omega}') \quad , \tag{1a}$$

where the surface condition for a general source $S(\boldsymbol{\rho})$ is

$$\phi(0,\boldsymbol{\rho},\boldsymbol{\Omega}) = S(\boldsymbol{\rho})\delta(\mu-\mu_0)\delta(\phi-\phi_0) \quad , \quad \mu_0 > 0 \quad , \tag{1b}$$

and the boundary conditions are

$$\lim_{z\to\infty}\phi(z,\boldsymbol{\rho},\boldsymbol{\Omega}) < \infty \quad , \quad \lim_{|\boldsymbol{\rho}|\to\infty}\phi(z,\boldsymbol{\rho},\boldsymbol{\Omega}) < \infty \quad . \tag{1c}$$

Schematic drawings of the coordinate systems and physical geometry are provided in Figures 1 and 2, respectively.

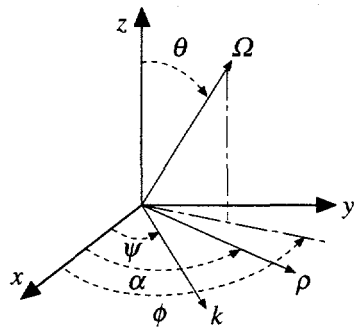

Fig. 1. Searchlight problem spatial and angular coordinate systems.

The source is normalized such that $\int d\boldsymbol{\rho}\, S(\boldsymbol{\rho}) = 1$. The solution method begins by taking a two-dimensional Fourier transform of the transport equation in the transverse ($\boldsymbol{\rho}$) plane, then progresses to the formation of integral expressions by following along particle trajectories. These integral expressions for the transform angular flux are then integrated over angle to produce the transformed scalar flux, given by

$$\bar{\Psi}(z;\boldsymbol{k}) = \bar{S}(\boldsymbol{k})\,e^{-z/U_0} + \frac{c}{2}\int_0^\infty dz'\,K(|z-z'|;\boldsymbol{k})\,\bar{\Psi}(z';\boldsymbol{k}) \quad , \tag{2a}$$

where we can show the kernel $K(z;\boldsymbol{k})$ to be[2]

$$K(z;\boldsymbol{k}) = \int_0^1 \frac{d\mu}{\mu}\,\frac{e^{-z(1+k^2\mu^2)^{1/2}/\mu}}{\left(1+k^2\mu^2\right)^{1/2}} \quad , \quad z > 0 \quad , \tag{2b}$$

$$U_0 = \frac{\mu_0}{u(\boldsymbol{\Omega}_0,\boldsymbol{k})} \quad , \tag{2c}$$

and

$$u(\boldsymbol{\Omega},\boldsymbol{k}) = 1 - ik\left(1 - \mu^2\right)^{1/2}\cos(\phi - \psi) \quad . \tag{2d}$$

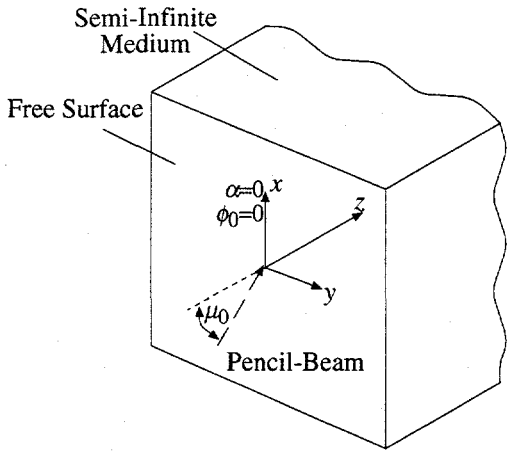

Fig. 2. Searchlight problem schematic drawing.

The solution to the transformed transport equation is accomplished by considering a corresponding one-dimensional pseudo transport equation.[2,3] The solution to the half-space pseudo problem is obtained by following the methods established by Busbridge[11] and detailed in Ref. 9. This solution and correspondence to the direct problem yields the following expression for the transformed scalar flux at the surface

$$\overline{\Psi}(0;\boldsymbol{k}) = \overline{S}(\boldsymbol{k})H(U_0;k) \quad , \tag{3}$$

where the H-function is given by the nonlinear integral equation

$$H(\xi;k) = 1 + \xi H(\xi;k)\,\frac{c}{2}\int_0^1 \frac{d\mu'}{1 + k^2\mu'^2}\,\frac{H(\xi';k)}{\xi' + \xi} \quad , \tag{4}$$

with $\xi(\mu) = \mu/(1+k^2\mu^2)^{1/2}$. When $k = 0$, Eq. (4) reduces to the standard H-function as derived by Chandrasekhar.[12] The Busbridge solution method also produces an expression for the interior pseudo scalar flux in terms of a Laplace transform. The Laplace transform, denoted by $\mathcal{L}_s\{\bullet\}$, of the interior transformed scalar flux is expressed as a function of the transformed surface scalar flux as[9]

$$\overline{\Psi}(z;\boldsymbol{k}) = \overline{S}(\boldsymbol{k})\; U_0\, H(U_0;k)\; \mathcal{L}_z^{-1}\left\{\frac{1}{1 + sU_0}\,H[1/s;k]\right\} \quad . \tag{5}$$

III. THE DIRECT SCALAR FLUX

The direct scalar flux is obtained by inverting the double Fourier transform, which is explicitly written as

$$\phi(z,\boldsymbol{\rho}) = \frac{1}{(2\pi)^2}\int_0^\infty dk\; k \int_0^{2\pi} d\psi\; e^{-ik\rho\cos(\psi-\alpha)}\;\overline{\Psi}(z;\boldsymbol{k}) \quad . \tag{6}$$

Upon substitution of the transformed surface and interior scalar fluxes, we have

$$\phi(0,\boldsymbol{\rho}) = \frac{1}{(2\pi)^2} \int_0^\infty dk\, k \int_0^{2\pi} d\psi\, e^{-ik\rho\cos(\psi-\alpha)}\, \bar{S}(\boldsymbol{k}) H(U_0;k) \;; \tag{7a}$$

$$\phi(z,\boldsymbol{\rho}) = \frac{1}{(2\pi)^2} \int_0^\infty dk\, k \int_0^{2\pi} d\psi\, e^{-ik\rho\cos(\psi-\alpha)} \bar{S}(\boldsymbol{k}) U_0 H(U_0;k)\, \mathcal{L}_z^{-1}\left\{\frac{H[1/s;k]}{1 + sU_0}\right\} \;. \tag{7b}$$

A significant simplification occurs if the anisotropic source impinges normal to the surface. In this case, $\mu_0 = 1$, which implies that $U_0 = 1$, and $\bar{S}(\boldsymbol{k})$ is a function of the magnitude of $\boldsymbol{k}$ only. The entire dependence on ψ in the kernels in the above formulations is lost except for the complex exponential; the integral over $d\psi$ then becomes the zeroth order Bessel function. Clearly if $\mu_0 = 1$ the scalar flux is two-dimensional. These cases have been previously treated numerically.[9] In general, however, $\mu_0 \neq 1$ and the scalar flux is three-dimensional.

IV. NUMERICAL METHODS

As is evident in Eqs. (7), the numerical solution for the scalar flux involves many procedures including H-function evaluation, a Laplace transform inversion, and a double Fourier transform inversion. Each numerical procedure will be discussed separately.

IV.A. Numerical Evaluation of the H-Function

The numerical evaluation of the H-function is essential to determining the scalar fluxes. The nonlinear integral equation to be solved is rearranged to give

$$H(\xi;k) = \left[1 - \xi \frac{c}{2} \int_0^{1/(1+k^2)^{1/2}} \frac{d\xi'}{(1 - k^2\xi'^2)^{1/2}} \frac{H(\xi';k)}{\xi' + \xi}\right]^{-1} \;. \tag{8}$$

A moment relation for the generalized H-function can also be derived as

$$\alpha_0 = \int_0^1 d\mu \frac{H(\xi;k)}{1 + k^2\mu'^2} = \frac{2}{c}\left[1 - \left(1 - c\frac{\tan^{-1}k}{k}\right)^{1/2}\right] \;. \tag{9}$$

The evaluation of the H-function is made simpler because the range of integration and the argument of the H-function inside the integrals are real. Thus, we use an iteration scheme to evaluate the real H-function in the range of integration, and then this "converged" H-function is used to generate the value of the general H-function for any ξ, which may be complex. The iteration scheme uses Gauss-Legendre quadrature of order L_m to evaluate the integrals; thus, an iteration is performed for each $H(\xi_m;k)$. The iteration process and the algebra of real and imaginary H-functions are detailed in Ref. 13.

IV.B. The Laplace Transform Inversion

Like the Fourier transform pair, the Laplace transform pair is composed of integrals in the complex plane. If the direct function, $f(t)$, is known to be real, then the inversion may be expressed as

$$f(t) = \frac{2e^{\gamma t}}{\pi} \int_0^\infty d\omega \cos(\omega t)\, \mathrm{Re}F(\gamma + i\omega) \;. \tag{10}$$

Physical quantities, such as a scalar flux, must be mathematically real to be of physical significance. However, a real integral does not imply that its integrand must also be real. For an integral to be real, either the integrand itself must be real or the imaginary part of the integrand must integrate to zero. The integrand for the interior scalar flux [Eq. (7b)] contains a Laplace transform inversion; however, this Laplace transform inversion is multiplied by a complex exponential and other complex quantities such as U_0 and $H(U_0;k)$. If the scalar flux is determined as shown in Eq. (7b), the result of the Laplace transform inversion (the direct function) will be complex, and therefore Eq. (10) may not be used for the Laplace transform inversion. If the integral over $d\psi$ is performed inside the Laplace transform inversion as

$$\phi(z,\boldsymbol{\rho}) = \frac{1}{(2\pi)^2} \int_0^\infty dk\ k\ \mathcal{L}_z^{-1}\left\{ H[1/s;k] \int_0^{2\pi} d\psi\, e^{-ik\rho\cos(\psi-\alpha)} \bar{S}(\boldsymbol{k})\, \frac{U_0 H(U_0;k)}{1 + sU_0} \right\} , \tag{11}$$

then Eq. (10) can be used for the Laplace transform inversion. For the interior scalar flux as given by Eq. (11) to be real for all z and $\boldsymbol{\rho}$, the integrand (i.e. the Laplace transform inversion) must also real.

IV.C. The Double Fourier Transform Inversion and the Scalar Flux

The double Fourier transform inversion is common to the surface and interior scalar fluxes. The inversion has the form

$$F(\boldsymbol{\rho}) = \frac{1}{(2\pi)^2} \int_0^\infty dk\ k \int_0^{2\pi} d\psi\, e^{-ik\rho\cos(\psi-\alpha)}\, \bar{F}(k,\psi) \ . \tag{12}$$

Fortunately, all H-functions in the integrands of the Fourier inversions are parameterized in k only. To examine the implications of this simplification, we consider the function $H(U_0;k)$. A converged H-function can be determined for a given k. U_0 is a function of ψ, but the same set of converged H-functions can be used for each ψ in the evaluation of $H(U_0;k)$. The iteration to determine the converged H-function may then be performed outside the integral over $d\psi$ with only the interpolation of the H-function to give $H(U_0;k)$ required inside the integral over $d\psi$.

The integral over dk in Eq. (12) is evaluated by converting the semi-infinite integral into an infinite series of finite integrals as

$$F(\boldsymbol{\rho}) = \frac{1}{(2\pi)^2} \sum_{j=0}^{\infty} \int_{a_j}^{a_{j+1}} dk\ k\ \bar{F}(k) \ , \tag{13}$$

where the a_j are points at which the integral over dk is partitioned. For a normal beam, the function $\bar{F}(k)$ contains a zeroth order Bessel function, and the a_j points are conveniently set to the zeros of $J_0(k)$; however, in general, a zero finding scheme, such as the bisection method, is used to determine the zeros of $\bar{F}(k)$ and these zeros are used as the points a_j. This produces a purely oscillating series that is amenable to Euler-Knopp[14] acceleration. The integrals over $d\psi$ are most efficiently performed using Chebyshev integration.

The only source considered in this study of the searchlight problem is a pencil-beam that impinges on the surface of the half-space at the origin. Thus, $S(\boldsymbol{\rho}) = \delta(\rho)/(2\pi\rho)$ and $\bar{S}(\boldsymbol{k}) = 1$. Extracting the particles that come directly from the source [by subtracting 1 from $H(U_0;k)$] is convenient and gives for a general source variation on the surface:

$$\phi(0,\boldsymbol{\rho}) = S(\boldsymbol{\rho}) + \frac{1}{(2\pi)^2} \int_0^\infty dk\ k \int_0^{2\pi} d\psi\, e^{-ik\rho\cos(\psi-\alpha)}\, [H(U_0;k) - 1] \ , \tag{14}$$

If the complex H-function is separated into real and imaginary parts and the complex algebra performed for the integrand in Eq. (14b), the surface scalar flux can be shown to be real, as it must be, and is given by

$$\phi(0,\rho) = \frac{\delta(\rho)}{(2\pi\rho)} + \frac{1}{2\pi^2}\int_0^{\infty} dk\ k \int_0^{\pi} d\psi \left\{ \cos(q)[H_R(U_0;k) - 1] + \sin(q)H_I(U_0;k) \right\} , \tag{15}$$

where $q = k\rho\cos(\psi - \alpha)$ and H_R and H_I are the real and imaginary parts of the H-function, respectively. When the beam is normal, $U_0 = 1$, $H_I = 0$, and the cosine term integrates to a zeroth order Bessel function to give the expected two-dimensional result.

Some simplifications in the expressions for the interior scalar flux can also be made by noting that the final result must be real. When the integral over $d\psi$ is performed inside the Laplace transform inversion, as in Eq. (11), the result of the inversion must be real for the scalar flux to be real. The interior scalar flux can be shown to be real by expressing complex factors in terms of their real and imaginary parts, collection the entire expression into real and imaginary parts, and showing the imaginary part to be zero. If the beam is normal to the surface, U_0 is 1, the integral of the complex exponential in Eq. (11) becomes $J_0(k\rho)$, and the two-dimensional form for the interior flux is recovered.

V. NUMERICAL RESULTS

V.A. The Scalar Flux at the Surface

The numerical evaluation of the surface scalar flux is obtained by using standard numerical techniques such as iterative Gauss-Legendre quadrature, Chebyshev integration, transformation of a semi-infinite integral into an infinite series, Euler-Knopp acceleration, and double inversions in Cartesian coordinates. The surface scalar flux is given by Eq. (7a). The required inversion contains a double integral, of which the outer integral is over the k variable and the inner integral is over ψ. With the converged values of the H-function calculated for each k, only one interpolative evaluation of the H-function at the particular ψ values associated with U_0 must be performed inside the integral over $d\psi$. As usual, the integral over dk, which has a semi-infinite range, is converted into an infinite series of integrals. The range of integration for these integrals may be the zeros of the zeroth order Bessel function or the zeros of the integrated function. In general, use of Gauss-Legendre quadrature or Romberg integration for the outer integrals and Chebyshev integration for the inner integrals is most efficient.

Some numerical results for the surface scalar flux are presented in Table I in the form of an error convergence analysis. The results were generated with a scattering coefficient of $c = 0.9$, an incident angle $\mu_0 = 0.7$, $\phi_0 = 0$ (hereafter, unless otherwise noted, the incident azimuthal angle is 0), and at $y = 0.1$. The numerical integration parameters include outer integration using variable Gauss-Legendre quadrature (where the integral is evaluated at successively higher quadrature orders until a prescribed number of consecutive integral evaluations are within a specified tolerance) with an initial quadrature of 10 and increment 2 (with iterative H-function evaluation), and an inner Chebyshev integration with initial quadrature 20 and increment of 20. The zeros of $J_0(k)$ are the endpoints of the finite outer integrals. The numerical values of the scalar flux agree with each other to the required number of significant digits based on the convergence criteria. Furthermore, the values of the scalar flux are greater at positive values of x than at negative values of x because of the canted beam introducing particles into the region of positive x.

Table I. Error Convergence Analysis for the Surface Scalar Flux

x	$err = 10^{-2}$	$err = 10^{-3}$	$err = 10^{-4}$	$err = 10^{-5}$	$err = 10^{-6}$
-2	4.424424E-3	4.425169E-3	4.425259E-3	4.425270E-3	4.425272E-3
-1.5	8.720801E-3	8.721863E-3	8.721989E-3	8.722005E-3	8.722007E-3
-1	1.965904E-2	1.967439E-2	1.967635E-2	1.967637E-2	1.967637E-2
-0.5	6.050579E-2	6.054166E-2	6.054566E-2	6.054619E-2	6.054618E-2
0	6.873938E-1	6.872902E-1	6.872764E-1	6.872741E-1	6.872742E-1
0.5	2.047136E-1	2.047531E-1	2.047594E-1	2.047592E-1	2.047591E-1
1	7.202231E-2	7.204633E-2	7.204537E-2	7.204524E-2	7.204522E-2
1.5	3.322871E-2	3.322389E-2	3.322325E-2	3.322315E-2	3.322315E-2
2	1.730579E-2	1.730218E-2	1.730159E-2	1.730162E-2	1.730162E-2

The surface scalar flux is primarily a function of two spatial variables (x,y) or (ρ,α), and one source parameter, μ_0. We now examine the scalar flux on the surface as a function of the spatial angle and source inclination. Such a plot is displayed in Figure 3. Figure 3 was generated at $c = 0.9$ and the scalar flux is converged to 10^{-4}. The scalar flux is shown as a function of α and μ_0 at $\rho = 1$. When $\mu_0 = 1$ (a normal beam) the scalar flux is independent of angle, as expected. When the incident beam is exactly grazing ($\mu_0 = 0$), the scalar flux is zero, and as μ_0 approaches zero the scalar flux does likewise. At small spatial angles, the scalar flux begins to increase as μ_0 decreases, peaks, and then decreases to zero. As the beam is canted, more particles are scattered into the areas that have small spatial angular coordinates, but eventually the beam is so canted that the effect of scattering more particles into the region with small spatial angular coordinates is overcome by the loss of particles through the surface. At large angles (α near 180°), when the beam is canted, it shines particles in a direction that is increasingly farther from the spatial point and therefore the scalar flux continuously decreases.

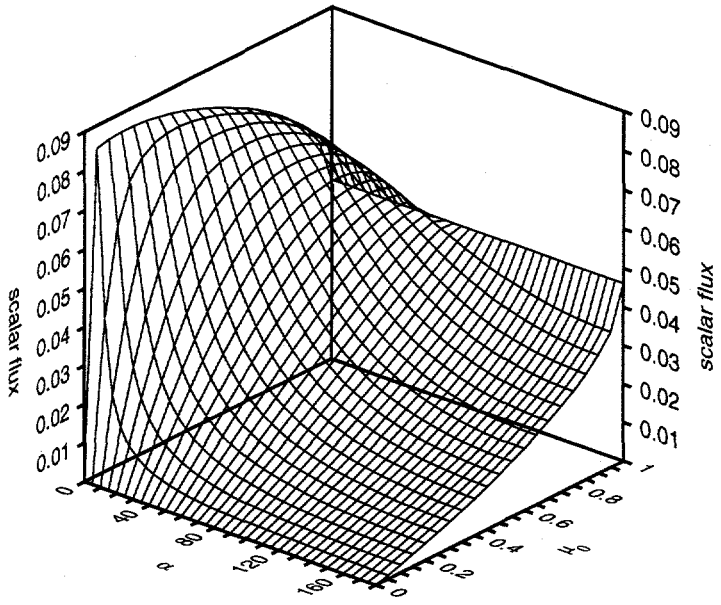

Fig. 3. The surface scalar flux as a function of positional angle (α) and beam incident angle (μ_0) at $\rho = 1$ with $c = 0.9$.

V.B. The Interior Scalar Flux

As with the scalar flux at the surface of the half-space, evaluation of the interior scalar flux requires evaluation of the H-function. However, the evaluation is further complicated by the need for a Laplace transform inversion inside the double Fourier inversion. With three embedded integrals to compute, along with an H-function iteration, efficient calculations are obtained when few or no iterations are performed. Without the confidence in the answer that comes from a solution that has used the iterative processes, some measure must be found to provide confidence in the numerical results of the calculation. This confidence is obtained primarily by testing the results at various quadrature orders, and by occasionally allowing the algorithm to iterate. When this testing is performed, the outer integral over dk is evaluated accurately by means of Gauss-Legendre quadrature at orders of 10 or 20. The inner integrals over $d\psi$ generally require Chebyshev quadrature orders of 50 for most problems; however, when c is small, higher quadrature orders are required.

One drawback to setting the quadrature orders and not allowing iteration is that the results are limited in their accuracy. The lowest relative error that can be achieved for most results (with any degree of confidence) is 10^{-4}. First, the time required to obtain this error is quite long, and second, the algorithm often becomes unstable if stricter errors are requested. The instability arises because the quadrature order of the inner integrals is set, and for large k, as required for evaluations at low relative errors, the quadrature order is not sufficient to provide an accurate determination of the function being integrated.

An error analysis of the results from calculating the interior scalar flux is provided in Table II. The physical and spatial parameters are $\rho = 1$, $\alpha = 30°$, $c = 0.9$, $\mu_0 = 0.9$. Generally, the inner integral over $d\psi$ uses a fixed Chebyshev quadrature order of 50. The average calculation time per point on a DEC alpha 3000 workstation with 64 MB of internal memory is listed at the bottom of the table. As usual, the results agree with each other to the required number of digits. The final column, listed also as being converged to a 10^{-4} error (with an asterisk) was allowed to iterate on both inner and outer integrals. The CPU time required to obtain results (180 min/point) reflects the computational effort required when additional inner iterations are allowed.

Table II. Error Convergence Analysis for the Interior Scalar Flux

z	$err = 10^{-2}$	$err = 10^{-3}$	$err = 10^{-4}$	$err = 10^{-4*}$
0.5	1.0828E-1	1.0823E-1	1.0825E-1	1.0825E-1
1	1.2466E-1	1.2446E-1	1.2445E-1	1.2449E-1
1.5	1.1289E-1	1.1281E-1	1.1282E-1	1.1281E-1
2	8.3406E-2	8.3359E-2	8.3361E-2	8.3347E-2
2.5	5.3373E-2	5.3358E-2	5.3352E-2	5.3355E-2
3	3.2717E-2	3.2738E-2	3.2741E-2	3.2742E-2
3.5	2.0357E-2	2.0337E-2	2.0338E-2	2.0339E-2
4	1.2961E-2	1.2953E-2	1.2952E-2	1.2952E-2
4.5	8.4463E-3	8.4454E-3	8.4452E-3	8.4451E-3
5	5.6201E-3	5.6172E-3	5.6167E-3	5.6166E-3
	216 sec.	444 sec.	939 sec.	10,800 sec.

Perhaps the most useful means of viewing the scalar flux comes as a contour plot in two spatial dimensions. A slice of the medium is taken parallel to the z-axis at a particular position y so that the canted nature of the beam is clearly visible. The variation in z begins at the free surface and extends to some point in the medium. Figure 4 displays a contour plot of the scalar flux versus x and z at $y = 0.5$. The spatial variable x ranges from [–2, 2] and z ranges from [0,5]. The beam impinges on the free surface of a $c = 0.9$ medium at an angle $\theta_0 = 25.8°$ ($\mu_0 = 0.9$). When the edit grid is near the source, the directed nature of the source is clearly visible as is the buildup peak inside the surface. As the edit grid moves farther from the source, the buildup peak moves into the medium and the directed nature of the source becomes less evident.

VI. COMPARISON WITH MCNP

Los Alamos National Laboratory has developed the MCNP[10] production-scale code for transport calculations. This code uses standard probabilistic Monte Carlo methods to follow particles throughout a specified geometry. A comparison of results from MCNP and the analytic solution is provided for an analysis of the canting angle of the incident beam. Figure 5 displays the effects of changing μ_0. Three spatial points are fixed [the points are $(x,y,z) = (1,0.5,1)$, $(2,0.5,1)$, and $(3,0.5,1)$] and the number of secondaries per collision is described by $c = 0.9$. As on the surface, the scalar flux rises from zero for a grazing beam ($\mu_0 = 0$), peaks at some μ_0 where the beam emits into a direction that passes near to the specified spatial point, and then decreases again as the beam direction moves away from the spatial point until it emits along the z-axis ($\mu_0 = 1$). The individual points displayed are the results of MCNP calculations using point detectors at the locations shown (error bars indicate +/– two standard deviations). One million particles were followed throughout a $60 \times 60 \times 30$ (x, y, z) mean-free-path medium. The medium consists of 90% purely scattering isotopes and 10% purely absorbing isotopes with a total cross section of 1.0. The standard deviations associated with the MCNP calculations ranged between 1 and 2%, with an approximate calculation time of 15 minutes on a Sparc 10 workstation with 64 MB of internal memory. Excellent agreement between the analytic solution and the established production-scale code is obtained; 51% and 90% of the MCNP data points in Figure 5 are within one and two standard deviations of the analytical values, respectively.

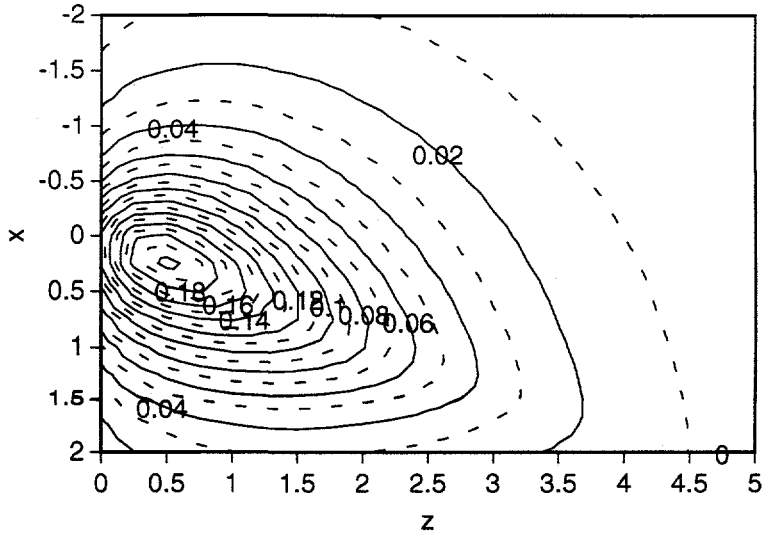

Fig. 4. Contour mapping of the interior scalar flux as a function of x and z for $c = 0.9$, $\mu_0 = 0.9$, and $y = 0.5$.

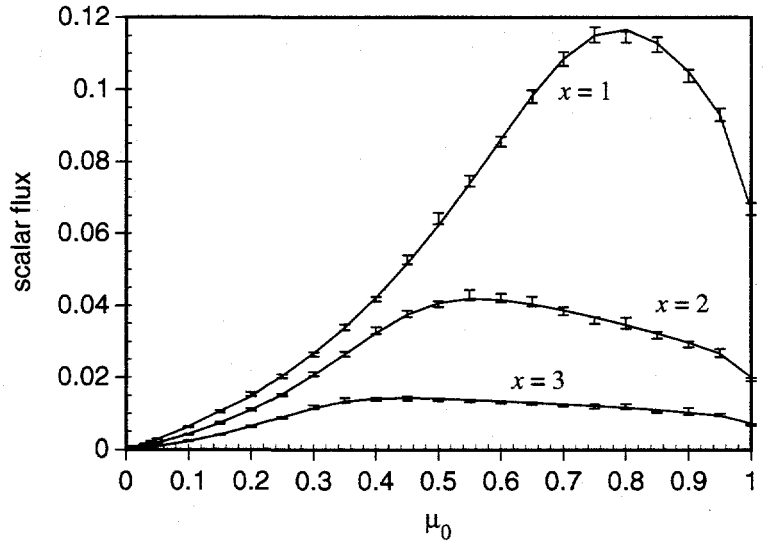

Fig. 5. Interior scalar flux as a function of μ_0 for three values of x at $z = 1$, $y = 0.5$, and $c = 0.9$. Displayed points are values obtained using MCNP.

VII. CONCLUSIONS AND RECOMMENDATIONS

The calculation of the scalar flux resulting from a canted beam impinging on the surface of a half-space, which involves integrals related to three inversions, requires a great deal of computational power and time to produce results. Results can be generated to an accuracy of 10^{-4} in a reasonable time for problems that are not highly absorbing and for beams that are not severely canted. However, given the nature of the inversions these calculations would have been impossible without the improved speed of computers that are now available in desktop workstations and personal computers. Ultimately, the future of analytical benchmarking lies in the use of parallel processing. The formulations are such that a minimal amount of parallel programming would allow individual processors to be devoted to separate evaluations of the integral expressions based on spatial or source parameters. Accomplishment of these tasks should be a part of a subsequent and consistent effort to provide more complex and realistic benchmarks for the nuclear, medical, astrophysical, and the earth sciences communities.

REFERENCES

1. S. CHANDRASEKHAR, "On the Diffuse Reflection of a Pencil of Radiation by a Plane-Parallel Atmosphere," *Proceedings of the National Academy of Science U.S.A.*, **44**, 933 (1958).

2. M. M. R. WILLIAMS, "The Three-Dimensional Transport Equation with Applications to Energy Deposition and Reflection," *J. Physics A: Math. Gen.*, **15**, 965 (1982).

3. G. B. RYBICKI, "The Searchlight Problem with Isotropic Scattering," *Journal of Quantitative Spectroscopy and Radiative Transfer*, **11**, 827 (1971).

4. C. E. SIEWERT and W. L. DUNN, "Radiation Transport in Plane-Parallel Media with Non-Uniform Surface Illumination," *J. Appl. Math. Phys.*, **34**, 627 (1983).

5. C. E. SIEWERT, "On the Singular Components of the Solution to the Searchlight Problem in Radiative Transfer," *J. Quant. Spect. Rad. Trans.*, **33**, 551 (1985).

6. C. E. SIEWERT and W. L. DUNN, "The Searchlight Problem in Radiative Transfer," *J. Quant. Spect. Rad. Trans.*, **41**, 467 (1989).

7. J. P. ELLIOTT, "Milne's Problem with a Point-Source," *Proceedings of the Royal Society (London)*, **A228**, 424 (1955).

8. B. D. GANAPOL and D. W. NIGG, "Analytical Two-Dimensional Neutron Transport Benchmark: The Searchlight Problem," *Trans. Am. Nuc. Soc.*, **64**, 276 (1991).

9. B. D. GANAPOL, D. E. KORNREICH, J. A. DAHL, D. W. NIGG, S. N. JAHSHAN, and C. A. WEMPLE, "The Searchlight Problem for Neutrons in a Semi-Infinite Medium," *Nucl. Sci. Engr.*, **118**, 38, (1994).

10. J. F. BRIESMEISTER, "MCNP - A General Monte Carlo N-Particle Transport Code," Los Alamos National Laboratory, LA-12625-M (1993).

11. I. W. BUSBRIDGE, *The Mathematics of Radiative Transfer*, Cambridge University Press, Cambridge (1960).

12. S. CHANDRASEKHAR, *Radiative Transfer*, Dover Publications, Inc., New York (1960).

13. KORNREICH, D. E., and B. D. GANAPOL, "Numerical Evaluation of the Three-Dimensional Searchlight Problem in a Half-Space," to be published in *Nucl. Sci. Engr.* (1997).

14. W. H. PRESS, *et al.*, *Numerical Recipes in FORTRAN, Second Edition*, Cambridge University Press, Cambridge (1992).